CrossMark

GYNECOLOGIC ONCOLOGY

Multi-scale hyperspectral imaging of cervical neoplasia

Chaojian Wang[1] · Wenli Zheng[1] · Yanggao Bu[2] · Shufang Chang[3] ·
Shiwu Zhang[1] · Ronald X. Xu[1,4]

Abstract

Purpose This preliminary study aimed at investigating the feasibility and effective of multi-scale hyperspectral imaging in detecting cervical neoplasia at both tissue and cellular levels.

Methods In this paper, we describe a noninvasive diagnosis method with a hyperspectral imager for detection and location of cervical intraepithelial neoplasia (CIN) at multiple scales. At the macroscopic level, the hyperspectral imager was applied to capture the reflectance images of the entire cervix in vivo at a series of wavelengths. At the microscopic level, the hyperspectral imager was coupled with a microscope to collect the transmittance images of the pathological slide. The collected image data were calibrated. A wide-gap second derivative analysis was applied to differentiate CIN from other types of tissue.

Results At both macroscopic and microscopic levels, hyperspectral imaging analysis results were consistent with those of histopathological analysis, indicating the technical feasibility of multi-scale hyperspectral imaging for cervical neoplasia detection with accuracy and efficacy.

Conclusion We propose a multi-scale hyperspectral imaging method for noninvasive detection of cervical neoplasia. Comparison of the imaging results with those of gold standard histologic measurements demonstrates that the hyperspectral diagnostic imaging system can distinguish CIN at both tissue and cellular levels.

Keywords Multi-scale hyperspectral imaging · Wide-gap second derivative · Cervical intraepithelial neoplasia (CIN) · Pathological

✉ Shiwu Zhang
  swzhang@ustc.edu.cn

✉ Ronald X. Xu
  xu.202@osu.edu

1 Department of Precision Machinery and Precision Instrumentation, University of Science and Technology of China, Hefei, Anhui 230027, China

2 The 105th PLA Hospital, Hefei, Anhui 230031, China

3 Chongqing Medical University, Chongqing 400010, China

4 Department of Biomedical Engineering, The Ohio State University, Columbus, OH 43228, USA

Introduction

Cervical cancer is the second most common cancer among women worldwide, and more than 80 % of all cervical cancer patients occur in developing countries. In China, it is estimated that there are 150,000 new cervical cancer cases and 80,000 deaths every year according to the statistical data from Chinese center for disease control and prevention [1]. Cervical cancer is often caused by the infection of a virus called human papillomavirus (HPV) [2, 3] which was detected in 93 % of cervical cancer [4], and it will be successfully prevented or cured when it is found early via screening procedure. Colposcopy is an important step for screening cervical intraepithelial neoplasia (CIN). Digital colposcopy is routinely performed for patients with positive Papanicolaou (Pap) smear results before and after applying dilute acetic acid and Lugol's iodine. The histopathological examination always serves as the final diagnosis for cervical neoplasia. Although a standard set of metrics has been established for the screening of cervical neoplasia in China, the actual screening methods have several disadvantages such as poor specificity, low sensitivity, and subjective appraisal,

Springer

leading to inaccurate diagnosis and additional burden to patients. The biopsy is invasive and only takes some samples, which may lead to some missing lesions and some unnecessary hurts for patients [5]. Therefore, an objective and accurate method for clinical assessment of cervical neoplasia is very critical for early diagnosis and efficient therapy. Optical spectroscopy has demonstrated its effectiveness during the detection of various malignancies, including gastric cancer [6], oral neoplasia [6, 7] and cervical cancer [8, 9]. Spectroscopy is a noninvasive technique to obtain functional characteristics of tissue such as oxygenation level. It can also obtain biological features of CIN. For example, Raman spectroscopy is a noninvasive optical tool under investigation for cancer detection [10], it can provide molecular fingerprints and has the feasibility to classify healthy and premalignant lesions of tissue [11] and to predict treatment response to concurrent chemoradiotherapy in cervical cancers [12]. Diffuse reflectance spectroscopy detects the absorption and scattering characteristics of biologic tissue by studying diffusion and reflection of light at different wavelengths. Light scattering is affected by tissue morphology, epithelial thickness, and collagen content, all of which constantly change with the progression of the disease. Light absorption is affected by tissue absorbers such as oxy- and deoxy-hemoglobin. Pinto designed a portable spectroscopic scanner for intra-operative margin assessment based on diffuse reflectance spectroscopy and intrinsic fluorescence spectroscopy [13].

Several studies have been carried out to evaluate spectroscopy method is during in vivo diagnosis of cervical neoplasia. For example, Mirabal et al. utilized reflectance spectroscopy to measure reflected light as a function of illumination wavelength, and classified tissue using empirical experience in 161 patients [14]; Mourant et al. and Wang et al. designed the optic fiber to detect cervical neoplasia [15, 16]. However, these point-to-point measurement methods have a limited accuracy for appropriate localization of the disease. Wide-field hyperspectral imaging can acquire the reflectance images of the entire cervix at different wavelengths, and can potentially highlight the suspicious area. It can achieve better specificity in comparison with point-to-point probing methods [17]. In a study of 111 women, Ferris et al. investigated hyperspectral imaging mode to achieve a sensitivity of 97 % and a specificity of 70 % [9]. However, the acquisition of the hyperspectral images data is time-consuming, as well as the processing procedure. Besides, the hyperspectral imaging systems are always costly and burdensome [18]. Therefore, it is clinically necessary to replace the bulky hyperspectral imaging systems with a low-cost and portable one.

The goal of this study is to determine the feasibility of hyperspectral imaging technique for noninvasive detection of cervical neoplasia at both tissue and cellular levels. In this paper, a hyperspectral imaging system is provided to acquire reflectance images of the entire cervix under Xenon lamp illumination. Tissue reflectance spectra are processed using a wide-gap second derivate algorithm. The wide-gap second derivate algorithm was developed and applied in biomedical imaging which can achieve wavelength-dimensionality reduction and effectively reduce the impact caused by background absorption and illumination [19]. Applying wide-gap second derivative analysis, cervical neoplastic area can be potentially detected with only several selected wavelengths, which allow fast and effective diagnosis and treatment.

Pathological examination for cervical neoplasia can be conventionally carried out by taking the cervical biopsy samples, and staining them to identify cells with abnormal morphology from normal cells. However, the detection of abnormal cells in stained samples with a microscope is one of exhausting and time-consuming tasks in pathology [20]. In addition, the pathologists have the operator-dependent subjectivity in evaluating the borderline of dysplastic cells. To eliminate these limitations, we also applied the hyperspectral imaging technique at the microscopic level for cytologic diagnosis. The hyperspectral imager was coupled with a microscope to collect the transmittance images of the pathological slide. The collected image data were calibrated. The developed wide-gap second derivative analysis was applied to distinguish cancerous cells from normal cells. Our initial clinical experiment demonstrated that the hyperspectral imaging technique has potential applications to detect cervical neoplasia at both macroscopic and microscopic scales.

Materials and methods

Hyperspectral imaging system

The hyperspectral imaging system is shown in Fig. 1a. An acousto-optic tunable filter (AOTF) hyperspectral imager (500–900 nm, Brimrose, Sparks, MD, USA) was used to acquire hyperspectral image data cube of the target area through an AOTF adapter that serves as an electronically tunable spectral bandpass filter. AOTFs can switch wavelengths within microseconds and have a higher switching speed than other dispersive devices such as conventional gratings and liquid crystal tunable filters (LCTFs) do [21]. Fairly uniform and broadband illumination was provided by a 500-W continuous Xenon light source. The reflectance image of cervical tissue was captured by a monochrome charged coupled device (CCD) camera (JAI Apparatus,
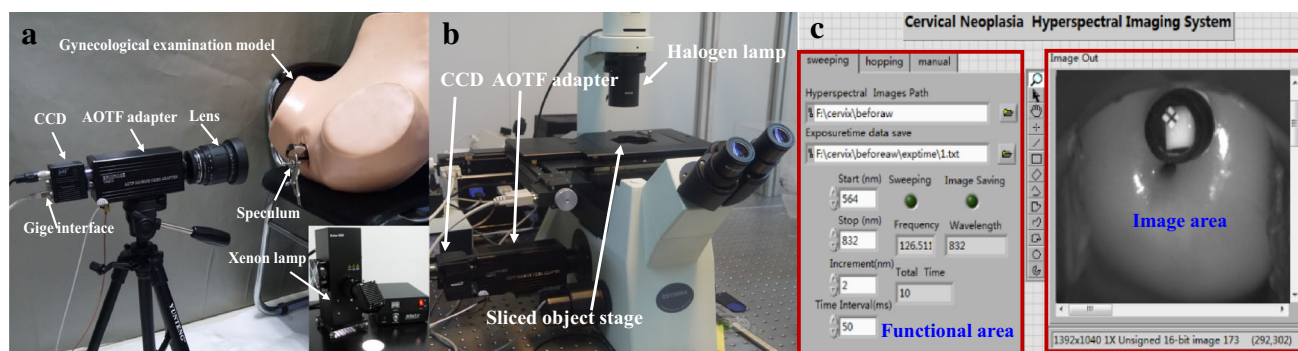
Fig. 1 **a** Hyperspectral imaging system developed for detection of cervical neoplasia; **b** hyperspectral microscopic imaging system; **c** LabVIEW interface programmed to control the system

Japan), which is a 16-bit, high-resolution imaging sensor (1392 × 1040 pixel with 6.45 um pixel size), and spectral responsivity range of the CCD matches that of the imager. Reflected lights pass through the camera lens to the AOTF adapter and finally produce images on the CCD. In the hyperspectral microscopic imaging system, a standard inverted fluorescence microscope (DSY5000X, Chongqing UOP Photoelectric Technology Corporation, China) was optically coupled with the AOTF adapter to collect the transmittance microscopic images at multiple wavelengths, as shown in Fig. 1b. The illumination of the microscope was provided by a halogen lamp. A LabVIEW interface as shown in Fig. 1c was programmed to control the hyperspectral system. Each reflectance spectrum ranges from 600 nm to 800 nm at an interval of 2 nm.

Spectral data normalization

The raw hyperspectral data were normalized by standardized methods including dark current subtraction and white reference normalization. To perform the normalization, a Teflon white board was placed to cover the whole field of view and the hyperspectral data were obtained. And the dark current was measured by covering the lens with a cap. The raw hyperspectral data were corrected by the following equation Eq. (1):

$$R(x, y, \lambda) = \frac{I_{\text{sample}}(x, y, \lambda) - I_{\text{dark}}(x, y, \lambda)}{I_{\text{white}}(x, y, \lambda) - I_{\text{dark}}(x, y, \lambda)} \quad (1)$$

where $R(x, y, \lambda)$ is the calculated relative reflectance of each wavelength, $I_{\text{sample}}(x, y, \lambda)$ is the raw radiance data of the sample, $I_{\text{dark}}(x, y, \lambda)$ is the dark current, and $I_{\text{white}}(x, y, \lambda)$ is the radiance value of the white board.

Clinical study

The clinical study protocol was approved by Institutional Review Board (IRB) of The Chongqing Medical University

(IRB No: 2013KLS002). Non-pregnant women with a positive result of ThinPrep Cytologic Test (TCT), which denotes a screening method to detect cervical abnormalities, were enrolled in the study. Biopsies were performed in 26 patients and six of them were verified being suffered from cervical neoplasia. Considering that it is a preliminary clinical test to demonstrate the multi-scale hyperspectral imaging's technical feasibility to detect CIN, the data of three representative subjects with different stages of neoplasia were selected to perform further multi-scale hyperspectral imaging analysis. When capturing the hyperspectral images of whole cervix, a speculum was inserted to expose the cervix completely. The hyperspectral imager was placed at a proper position to optimize focus after the surface of cervix was cleaned, as shown in Fig. 1a. A round container within a 4 mm × 4 mm white polytetrafluoroethylene (PTFE) board was placed on the surface of cervix. The PTFE board, with near unity reflectance, was calibrated by a NIST standard reference material (SRM) 2044, a traceable white diffuser (NIST, Gaithersburg, MD, USA), which reflected 99 % light in this wavelength range. The hyperspectral images were acquired from 600 to 800 nm at a spectral resolution of 2 nm. CCD's exposure time at each wavelength was continuous adjusted by the program automatically for the designated optical intensity. A series of reflectance images of cervix were then obtained according to the corresponding exposure time. Each pixel in the hyperspectral image has a sequence of reflectance in various spectral wavelengths and the sequence shows the spectral signature of that particular pixel. AOTF technology could switch wavelengths within microseconds, and combined with Gige interface can acquire image data rapidly. During the clinical test, women tolerated these procedures well and no adverse events reported. After hyperspectral scan, the cervix was then applied with diluted solution (3–5 %) of acetic acid for the purpose of visualization of neoplastic lesion, and the epithelium was whitened because of the intracellular dehydration and

coagulation of proteins [8]. Then the cervical surface was smeared with Lugol's iodine solution. The aceto-whitening and iodine-stained images were obtained by clinical digital colposcope (SLC-1000B, Goldway Apparatus, China) for initial diagnosis purpose. Upon completion of hyperspectral scan and conventional colposcopic examination, cervical biopsies were performed on suspected lesions and in some cases on normal areas if necessary.

Hyperspectral imaging of pathologic slides

For each patient recruited in this study, cervical tissue was biopsied at four suspicious sites, located at 3, 6, 9, and 12 o'clock approximately. The exact locations of the biopsies were indicated on the colposcopic color image by a surgeon. All the biopsy procedures were carried out by the same surgeon. These samples were then processed by a standard clinical procedure. Each biopsy sample was cut as two transverse sections synchronously to ensure the identical morphologic characteristics. One section was stained for conventional histopathological examination, the other was not stained to preserve the original tissue characteristics for hyperspectral microscopic imaging. Two kinds of calibration images were collected to normalize the spectrum: the dark images and the transmittance images of a neutral density filter. The same second derivative analytic methods as those on tissue level were applied to find the differences between normal and neoplastic tissue at the cellular level. Pathologic results were interpreted by the same pathologist at each biopsy site. Figure 2 presents the multi-scale cervical tissue images. Figure 2a was captured by a conventional colposcopy before application of acetic acid, Fig. 2b was captured by the hyperspectral imaging system at 650 nm, before acetic acid application. The PTFE board was used for data calibration and the cross marker on the board was for optimizing the focus. Figure 2c shows the pathological slide that was stained with H&E, the unstained pathological slide is shown in Fig. 2d, which was captured by our hyperspectral microscope imaging system at 650 nm. These two slides have the approximate morphological characters; however, because the unstained slide was non-deparaffinated, there were also some morphological differences between two images.

Wide-gap second derivative analysis

After the hyperspectral images of cervical tissue were obtained, the raw data were normalized by the white board in consideration of the different sensitivity and shutter speed of camera in various wavelengths. However, it is difficult to determine the differences between normal and neoplastic tissue only depending on the normalized reflectance because of the non-uniform radiation and tissue

scattering. Second derivative analysis can show some peaks that can be used to describe the characteristics of different objects due to lesion. The method was employed to enhance differentiations between normal and neoplastic area at both tissue and cellular level. Hence, the second derivative reflectance (SDR) analysis were performed to improve the analytic sensitivity and extract the biological features from the original spectra, meanwhile, the derivatives could also eliminate background signals [22]. SDR value can be calculated by the following equation Eq. (2):

$$SDR_{\lambda_i} = \frac{d^2 R}{d\lambda^2} = R_{\lambda_i + \Delta\lambda} + R_{\lambda_i - \Delta\lambda} - 2R_{\lambda_i} \tag{2}$$

where SDR_{λ_i} is the second derivative reflectance between $\lambda_{i-\Delta\lambda}$ and $\lambda_{i+\Delta\lambda}$, R_{λ_i}, $R_{\lambda_{i-\Delta\lambda}}$ and $R_{\lambda_{i+\Delta\lambda}}$ are the reflectance of λ_i, $\lambda_{i-\Delta\lambda}$ and $\lambda_{i+\Delta\lambda}$, respectively, $\Delta\lambda$ is the gap between λ_i and $\lambda_{i+\Delta\lambda}$.

The wavelength gap ($\Delta\lambda$) is an important parameter in data processing and determines the classification results directly. For finding an optimal $\Delta\lambda$, we selected 5–7 ROIs on the spectral image for every different tissue type as training sample based on the correct pathological results and biopsy location, and calculated their SDR values when the gap is from 2 to 90 nm. We found that when $\lambda_i = 690$ nm and $\Delta\lambda = 62$ nm, the inter-class distance of SDR values was maximal and the intra-class variance of SDR values was minimal.

So three raw spectral images (690, 690 ± 62 nm) were processing through Eq. (2), and we can achieve a computed SDR image. The image was further segmented to generate a diagnosis result through minimum Euclidean distance algorithm. The main formula of this algorithm can be described below:

$$D_{Ex} = \sqrt{\sum_{i=1}^{p} (R_{si} - R_{ti}^x)^2} \tag{3}$$

$$C_x = \min(D_{Ex}) \tag{4}$$

where R_{si} is the wide-gap second derivative value of each pixel of the computed SDR image and R_{ti}^x is the training data of different tissue types. D_{Ex} indicates the Euclidean distance calculated by R_{si} and R_{ti}^x. C_x indicates that the R_{si} is classified to the corresponding category by evaluating the minimum value D_{Ex}.

To verify the feasibility of hyperspectral imaging technique and the classification method at cellular level, the hyperspectral imaging system was also applied in biomedical field from microscopic perspective, the second derivative transmittance (SDT) analysis were performed and the same classification method was applied to analyze the cellular hyperspectral data. Compared to the tissue data, the preliminary results are consistent with the observation we made at the macroscopic level. The main steps of our whole spectral analysis are presented in Fig. 3.

Fig. 2 Multi-scale cervical tissue images: **a** colposcopic image; **b** hyperspectral image of cervical tissue at 650 nm; **c** ordinary microscopic image of stained cervical tissue slide; **d** hyperspectral microscopic image of unstained cervical tissue slide
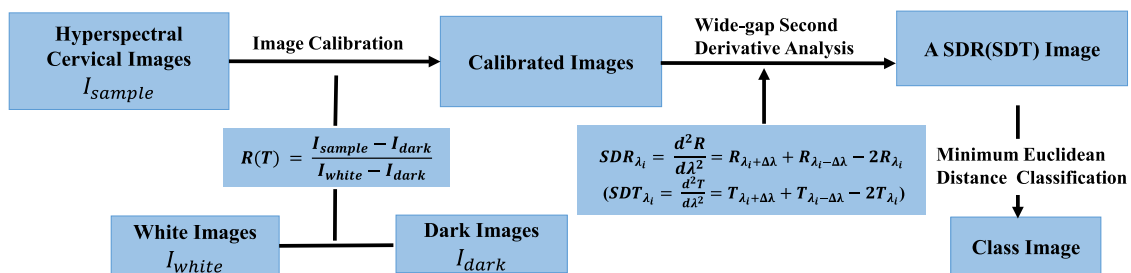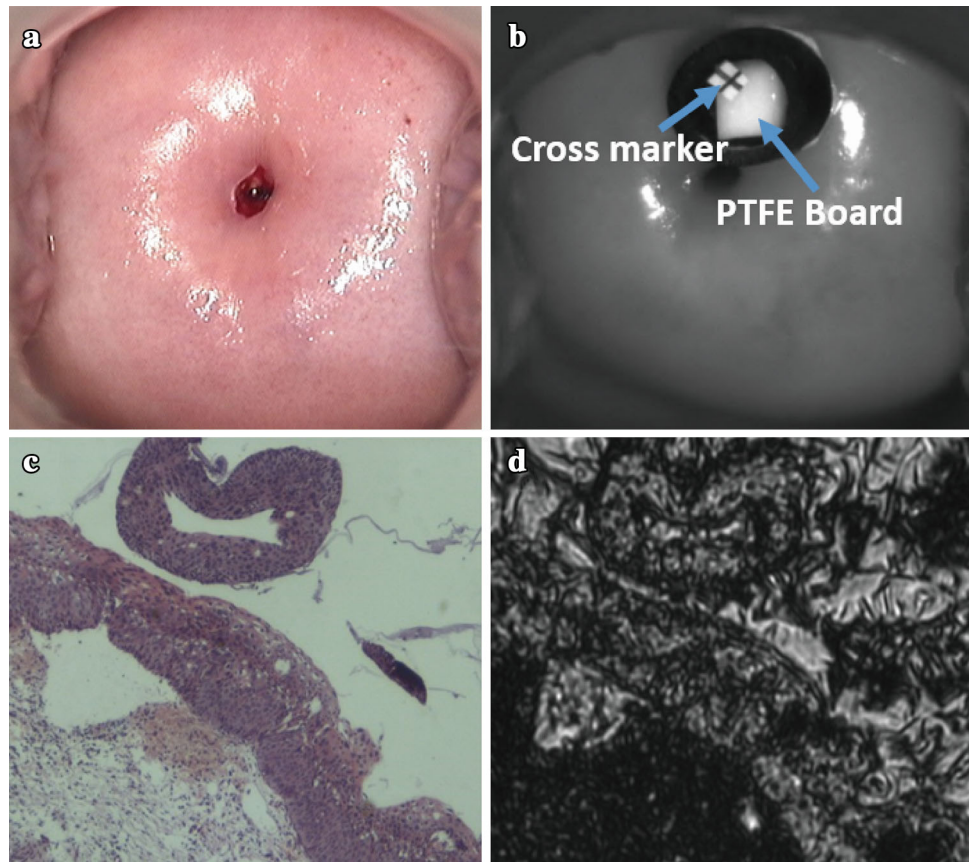

Fig. 3 Flowchart of the cervical tissue classification method by hyperspectral imaging

$$R(T) = \frac{I_{sample} - I_{dark}}{I_{white} - I_{dark}}$$

$$SDR_{\lambda_i} = \frac{d^2R}{d\lambda^2} = R_{\lambda_i+\Delta\lambda} + R_{\lambda_i-\Delta\lambda} - 2R_{\lambda_i}$$

$$(SDT_{\lambda_i} = \frac{d^2T}{d\lambda^2} = T_{\lambda_i+\Delta\lambda} + T_{\lambda_i-\Delta\lambda} - 2T_{\lambda_i})$$

Results

The captured hyperspectral images at both macroscopic (tissue) and microscopic (cellular) levels were preprocessed and analyzed by the above spectral analysis method. The performance of the method was also evaluated by experienced surgeon and pathologist. All image processing steps were carried out in Matlab software (Mathworks Inc., Natick, MA, USA) by the authors.

Cervical neoplasia is conventionally subdivided into 3 categories CIN1, CIN2, CIN3, according to the pathological findings [23]. CIN 3 is sometimes called high-grade or severe dysplasia. Figure 4 shows results from one patient

with CIN 3. Figure 4a shows the normalized reflectance spectra of normal (blue line), and neoplastic site (red line) of the 2 square dots in Fig. 4d, which are marked in blue (normal) and red (CIN3), respectively, the differences of spectral signatures in normal and abnormal cervical epithelia are consistent in all case. Figure 4b shows the corresponding wide-gap SDR curve of the reflectance described in Fig. 4a, the wavelength gap is 62 nm. According to the calculation of a large number of sites, one can find the second derivate spectra of neoplastic sites are similar, but are distinct from other sites. The results were then embedded to Euclidean distance classification method to create a false color map to spatially locate the cervical
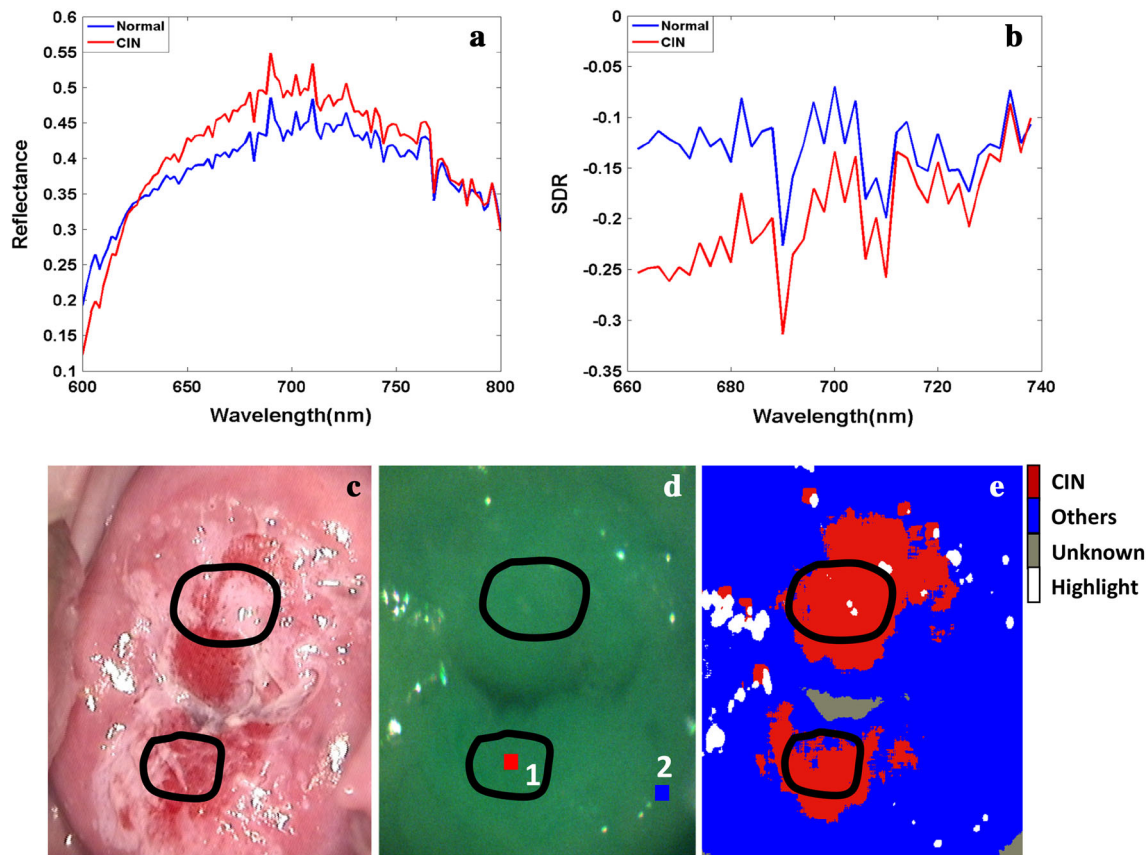
Fig. 4 Image classification results using wide-gap SDR method. **a** The relative reflectance curve of tissue in two different sites. **b** Corresponding wide-gap SDR spectra. **c** Colposcopic cervical image of an abnormal cervix with CIN 3 at 6 o'clock and 12 o'clock after application of acetic acid. *Black circle* the suspicious disease neoplasia. Figure 4c is obtained by a digital colposcopy after acetic acid application; the black circles which marked the most suspicious regions were drawn by an experienced surgery doctor, biopsy sites also performed in this area. Figure 4d is a pseudocolor map compound by three hyperspectral images before acetic acid application. Figure 4e shows the corresponding classification result based on the method, the hyperspectral reflectance images before acetic acid application were classified into several parts, where red region represents CIN 3 lesion area. Compared with the biopsy results—CIN 3 at 6 o'clock and 12 o'clock—the classification method correctly identifies the biopsied normal and neoplastic cervical tissue.

Figure 5 shows classification results adopted different methods. Figure 5a shows the result only using minimum Euclidean distance classification, and Fig. 5b shows the result using SDR analysis before minimum Euclidean distance classification. Comparing two classification results and combining with the biopsy results demonstrate that hyperspectral wide-gap second derivative analysis is effective to detect CIN.

areas identified by the clinician, biopsy sites also performed in this area. **d** Pseudo color map compound by three hyperspectral images. **e** Classification result depending on wide-gap SDR method combined with segmentation algorithm

Our hyperspectral microscopic experiment also showed some interesting preliminary results. The pathology slides without staining were scanned by the hyperspectral microscopic imaging system. A neutral density filter was used to normalize the transmittance spectra. Figure 6 shows some results from a single sample of unstained slide. Figure 6a shows the relative transmittance spectra of 2 different types of tissue. Figure 6b shows the corresponding wide-gap SDT curve of the transmittance described in Fig. 6a. Figure 6c is obtained by an inverted microscope, the black regions were marked by an experienced pathologist as the suspicious area of dysplasia. Figure 6d shows the corresponding classification result based on the SDT method combined with Euclidean distance classification algorithm. Minor false-positive results are also shown in the image, possibly caused by dirt and other artifacts of the unsealed and unstained slides. The microscopic hyperspectral imaging method described above may provide imaging guidance for pathologists before the pathologic diagnosis of neoplasia.

Fig. 5 Classification results depended on different methods. **a** The result is obtained by a minimum Euclidean distance algorithm directly; **b** The result is calculated by an SDR analysis before minimum Euclidean distance classification
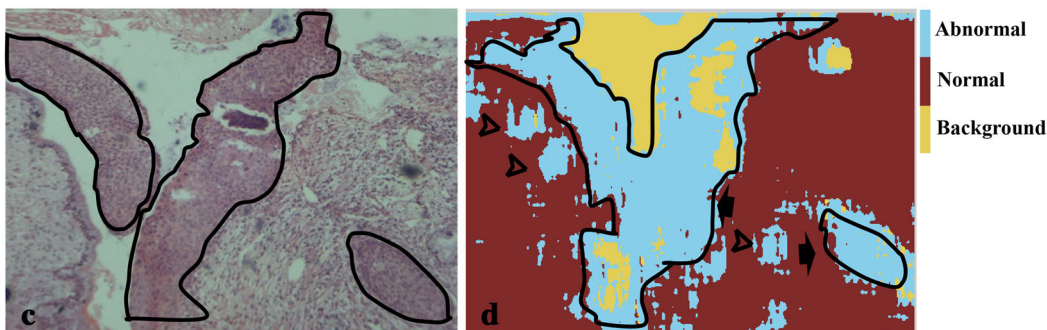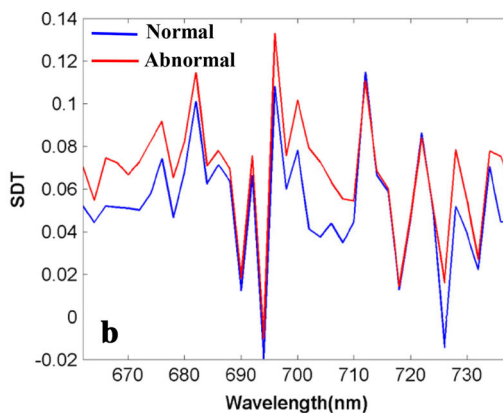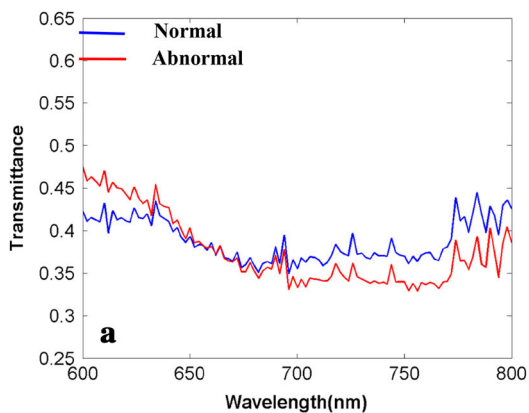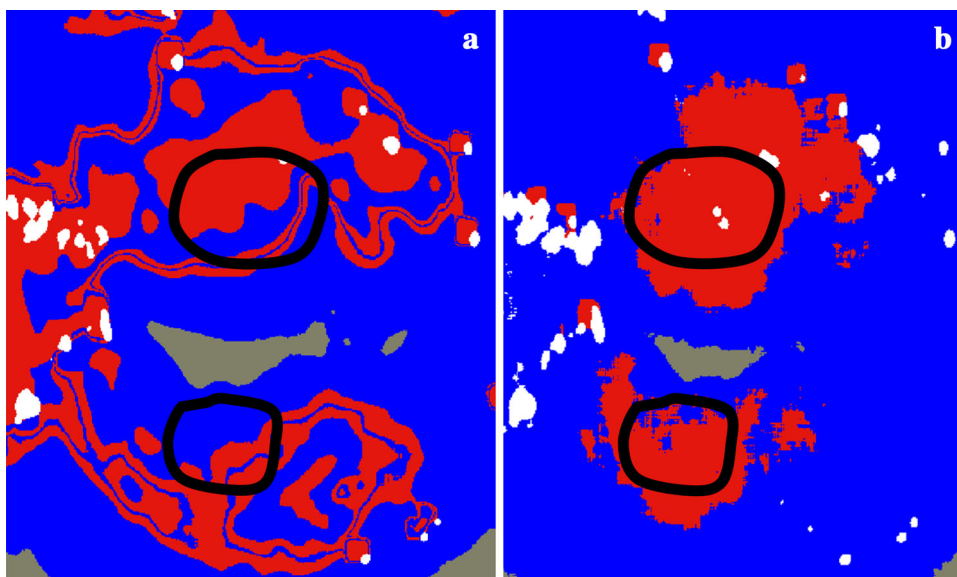

Fig. 6 Classification result of a pathology slide using based on wide-gap second derivative analysis: **a** the mean transmittance curve of tissue in 2 different areas; **b** corresponding wide-gap SDT spectra; **c** the H&E-stained histological slide shows cancer tissue as outlined by *black line*. **d** Classification result according to wide-gap SDT method combined with segmentation algorithm. Most of the cancer tissue (*arrows*) was detected using the method, while minor and false-positive areas are also shown (*arrowheads*)

Discussion

In this study, we have employed an AOTF hyperspectral imaging system and an advanced image processing algorithm to detect early cervical neoplasia at both tissue and cellular levels. In a clinical trial, an in vivo spectro imaging method was applied to differentiate various tissue types based on tissue reflectance spectrum, and an in vitro microscopic imaging method was applied to differentiate various cell types based on transmittance spectrum of

pathological slides. The preliminary results indicate that the hyperspectral imaging technique combined with wide-gap second derivative analysis could detect cervical neoplasia at different scales. The similar results between the two scales demonstrate the existence of biomarkers in cervical tissue, although the biochemical descriptions of them are difficult and uncertain, and demonstrate the unity between organism and cell. Our in vivo experiment has shown the differences between two mean SDR curves which are caused by the different sizes of cell nucleus in different tissue types, which is indicated by our hyperspectral microscopic experiment.

Considering that patients with cervical precancerous lesions may have a great chance to survive if the disease is diagnosed and treated early, the proposed multi-scale hyperspectral imaging technique has many potential applications with significant clinical impact over the conventional colposcopy methods: (1) diagnosis results are objective and potentially quantitative to determine the lesion margin at both tissue and cellular levels; (2) the screening procedure based on the technique can be performed noninvasively, compared with tissue biopsy; (3) our imaging system can detect neoplastic tissue in a larger area of cervix with a higher spatial resolution, while biopsy specimens can only be taken at a few sampling sites; (4) our classification method can acquire the diagnosis instantly, while patients will wait for a few days for conventional pathological examination results, owing to the time-consuming procedure of sample preparation, staining, and analysis.

Furthermore, hyperspectral imaging also has a tremendous potential to detect important molecular biomarkers of early cancers depending on their particular spectral characteristics. Recently, most groups use the wavelength bands from 400 to 700 nm to measure tissue neoplasia approximatively, because hemoglobin is the primary tissue absorber in the visible range. All the acquired reflectance spectra show valleys due to hemoglobin absorption at 420, 542 and 577 nm [14, 24–26]. However, the slope of the above 620 nm part of reflectance spectra become flat and no further relevant spectral features could be distinguished, there are also no significant and obvious characteristic peaks in raw reflectance spectra between normal and neoplastic tissue. Generally, oxygenated hemoglobin has a lower extinction coefficient between 650 and 750 nm. Within this range, the variation in content of oxygenated hemoglobin in various types neoplasia can significantly induce different reflectance spectrum. Our wide-gap second derivative method can enhance the resolution for the separation of overlapping peaks and the emphasis of small peaks [27] and identify the optimal bands from the whole spectrum [22]. Wide-gap second derivative is a suitable method to enhance

the differences and details and select several optimal bands to identify neoplasia.

In the recent years, some groups have investigated the clinical effectiveness of fluorescence spectra or the combination of fluorescence and reflectance spectra [25]. Meanwhile, several groups have focused on the change of spectral signatures after the application of acetic acid. Applying acetic acid will affect the reflectance measurement significantly [28], owing to the temporal alteration of the scattering properties of abnormal epithelium. After applying acetic acid, the epithelium scattering coefficient of neoplastic tissue is much higher than that of normal tissue [29]. Although our current study was based on the pure spectral characteristics of cervical tissue without applying acetic acid, it is possible to combine reflectance spectra with fluorescence spectra and spectral changes in response to acetic acid to improve the specificity and sensitivity of the system.

Compliance with ethical standards

Conflict of interest None.

References

1. http://www.chinacdc.cn/mtdx/mxfcrxjbxx/201405/t20140513_969 10.htm. Accessed 2014

2. Walboomers JMM, Jacobs MV, Manos MM et al (1999) Human papillomavirus is a necessary cause of invasive cervical cancer worldwide. J Pathol 189:12–19. doi:10.1002/(sici)1096-9896(199909)189:1<12:aid-path431>3.0.co;2-f

3. Barreto CL, Martins DBG et al (2013) Detection of Human Papillomavirus in biopsies of patients with cervical cancer. Arch Gynecol Obstet 288(3):643–648. doi:10.1007/s00404-013-3042-2

4. Bosch FX, Manos MM, MunB G et al (1995) Prevalence of human papillomavirus in cervical cancer: a worldwide perspective. J Natl Cancer Inst 87:796bste

5. Orfanoudaki IM, Kappou D, Sifakis S (2011) Recent advances in optical imaging for cervical cancer detection. Arch Gynecol Obstet 284(5):1197–1208. doi:10.1007/s00404-011-2009-4

6. Akbari H, Uto K, Kosugi Y et al (2011) Cancer detection using infrared hyperspectral imaging. Cancer Sci 102:852–857. doi:10.1111/j.1349-7006.2011.01849.x

7. Roblyer D, Kurachi C, Gillenwater AM et al (2009) In vivo fluorescence hyperspectral imaging of oral neoplasia. Proc SPIE 7169, 71690J-1–10

8. Gustafsson UP, McLaughlin E, Jacobsen E et al (2003) In-vivo fluorescence and reflectance imaging of human cervical tissue. Proc SPIE 5031:521–530

9. Ferris DG, Lawhead RA, Dickman ED et al (2001) Multimodal hyperspectral imaging for the noninvasive diagnosis of cervical

neoplasia. J Lower Genital Tract Dis 5:65–72. doi:10.1046/j.1526-0976.2001.005002065.x

10. Zeng H, Zhao J, Short M et al (2008) Raman spectroscopy for in vivo tissue analysis and diagnosis, from instrument development to clinical applications. J Innov Opt Health Sci 1(1):98–106. doi:10.1142/S1793545808000054

11. Singh SP, Deshmukh A, Chaturvedi P et al (2012) *In vivo* Raman spectroscopic identification of premalignant lesions in oral buccal mucosa. J Biomed Opt 17(10):1050021–1050029. doi:10.1117/1.JBO.17.10.105002

12. Rubina S, Vidyasagar MS, Murali KC (2013) Raman spectroscopic study on prediction of treatment response in cervical cancers. J Innov Opt Health Sci 6(2):1350014. doi:10.1142/S1793545813500144

13. Pinto F, Mielewczik M, Liebisch F et al (2013) Non-invasive measurement of frog skin reflectivity in high spatial resolution using a dual hyperspectral approach. PLoS One 8(9):e73234. doi:10.1371/journal.pone.0073234

14. Mirabal YN, Chang SK, Atkinson EN et al (2002) Reflectance spectroscopy for in vivo detection of cervical precancer. J Biomed Opt 7(4):587–594. doi:10.1117/1.1502675

15. Mourant JR, Bocklage TJ, Powers TM et al (2007) *In vivo* light scattering measurements for detection of precancerous conditions of the cervix. Gynecol Oncol 105:439–445. doi:10.1016/j.ygyno.2007.01.001

16. Wang A, Nammalavar V, Drezek R (2007) Targeting spectral signatures of progressively dysplastic stratified epithelia using angularly variable fiber geometry in reflectance Monte Carlo simulations. J Biomed Opt 12(4):044012. doi:10.1117/1.2769328

17. Tabrizi SH, Aghamiri SMR, Farzaneh F et al (2014) The use of optical spectroscopy for in vivo detection of cervical pre-cancer. Lasers Med Sci 29:831–845

18. Roblyer D, Park SY, Richards-Kortum R et al (2007) Objective screening for cervical cancer in developing nations: lessons from Nigeria. Gynecol Oncol 107:S94–S97. doi:10.1016/j.ygyno.2007.07.042

19. Karpińska J (2012) Derivative spectrophotometry-recent applications and directions of developments. Talanta 64(4):801–822

20. Wachman ES, Geyer SJ, Recht JM et al (2014) Simultaneous imaging of cellular morphology and multiple biomarkers using an acousto-optic tunable filter-based bright field microscope. J Biomed Opt 19(5):0560061–05600614. doi:10.1117/1.JBO.19.5.056006

21. Stratis DN, Eland KL, Carter JC et al (2001) Comparison of acousto-optic and liquid crystal tunable filters for laser-induced breakdown spectroscopy. Appl Spectrosc 55(8):999–1004

22. Becker BL, Lusch DP, Qi J (2005) Identifying optimal spectral bands from in situ measurements of Great Lakes coastal wetlands using second-derivative analysis. Remote Sens Environ 97:238–248. doi:10.1016/j.rse.2005.04.020

23. Fabrizii M, Moinfar F, Jelinek HF et al (2014) Fractal analysis of cervical intraepithelial neoplasia. PLoS One 9(10):e108457. doi:10.1371/journal.pone.0108457

24. Nordstrom RJ, Burke L, Niloff JM et al (2001) Identification of cervical intraepithelial neoplasia (CIN) using UV-excited fluorescence and diffuse-reflectance tissue spectroscopy. Lasers Surg Med 29:118–127. doi:10.1002/lsm.1097

25. Chang SK, Mirabal YN, Atkinson EN et al (2005) Combined reflectance and fluorescence spectroscopy for in vivo detection of cervical pre-cancer. J Biomed Opt 10(2):024031. doi:10.1117/1.1899686

26. Thekkek N, Richards-Kortum R (2008) Optical imaging for cervical cancer detection: solutions for a continuing global problem. Nat Rev Cancer 8(9):725–731. doi:10.1038/nrc2462

27. Morimoto S, McClure WF, Stanfield DL (2001) Hand-held NIR spectrometry: Part I: an instrument based upon gap-second derivative theory. Appl Spectrosc 55(2):182–189

28. Balas C (2001) A novel optical imaging method for the early detection, quantitative grading, and mapping of cancerous and precancerous lesions of cervix. Biomed Eng IEEE Trans 48(1):96–104. doi:10.1109/10.900259

29. Collier T, Follen M, Malpica A et al (2005) Sources of scattering in cervical tissue: determination of the scattering coefficient by confocal microscopy. Appl Opt 44(11):2072–2081. doi:10.1364/AO.44.002072